

# Quantum behavior in nanoscale ballistic rectifiers and artificial materials

A. Löfgren,<sup>1</sup> I. Shorubalko,<sup>1</sup> P. Omling,<sup>1</sup> and A. M. Song<sup>1,2,\*</sup>

<sup>1</sup>*Solid State Physics and Nanometer Consortium,  
Lund University, 221 00 Lund, Sweden*

<sup>2</sup>*Department of Electrical Engineering and Electronics,  
UMIST, Manchester M60 1QD, UK*

(Dated: November 1, 2018)

## Abstract

Low-temperature experiments are performed on novel nanoscale nonlinear devices (ballistic rectifiers) as well as nano-structured artificial materials, fabricated from an InP/InGaAs quantum well wafer. A DC output is generated between the lower and upper contacts of these devices, when an AC voltage is applied between the left and right contacts. As the temperature is lowered from room temperature, the DC output voltage of the ballistic rectifiers gradually changes from negative to positive. Since the negative output at high temperatures has been well understood in the framework of the classical ballistic electron transport, our results indicate that the electron transport comes into a new physical regime at low temperatures. Furthermore, we find that at even lower temperatures, the devices generate a pronounced oscillatory output as a function of the applied bias. Very similar phenomena are observed in the artificial nanomaterials, suggesting the existence of a common mechanism. We present a simple model based on quantum transport, which explains the key phenomena that we have observed at low temperatures.

PACS numbers: 73.23.Ad, 73.50.Fq, 73.40.Ei, 81.05.Zx

The rapidly advancing nanotechnology has made it possible to fabricate devices that are smaller than the electron mean free path,  $l_e$ . In these devices, electrons are mainly scattered at device boundaries rather than by randomly distributed scatterers such as impurities and phonons, and it is the device geometry that largely determines the paths traced by the electrons and, hence, the electronic properties. Based on this so-called ballistic electron transport, new device functionalities can be generated by simply tailoring the device shape. Although most studies on the ballistic electron transport were carried out in the linear regime,<sup>1</sup> more and more attention is paid to the non-linear regime.<sup>2,3,4,5,6,7,8,9,10</sup> Recently, it was also realized that the symmetry of the device geometry can have a pronounced influence on the nonlinear device properties.<sup>2,3,4,5</sup> One such example is the recently realized ballistic rectifier, in which a triangular antidot was fabricated in a ballistic micrometer-sized cross junction.<sup>3</sup> The triangular antidot breaks the symmetry of the device, and also serves as an artificial scatterer, which deflects the ballistic electrons to a certain direction independent of the direction of the applied electric field. The generated rectifying functionality has been shown to be so strong that when ballistic transport was realized at room temperature by fabricating nanometer-sized ballistic rectifiers, the sensitivity of microwave detection was found to be roughly as high as a commercial microwave diode.<sup>11</sup> Based on a similar working principle, artificial functional materials have been made by fabricating an array of nanometer-sized triangular antidots. The obtained nanomaterials have also been demonstrated to operate at room temperature and at frequencies up to at least 50 GHz.<sup>12</sup>

Apart from the promising potentials for real applications, the ballistic rectifiers and the nanomaterials might produce pronounced quantum effects at low temperatures. This is because the width of the channels, from which the ballistic electrons are ejected, is comparable to the electron Fermi wavelength. From the physics point of view, studying the influence of geometric symmetries of nanodevices on the quantum electron transport in the nonlinear regime is important, and only very limited number of such experiments have been reported.<sup>4,5,13</sup> In this work, we report on temperature-dependent experiments performed on the nanometer-sized ballistic rectifiers and nanomaterials. Surprisingly, reversed as well as oscillatory output is observed when the temperature,  $T$ , is sufficiently lowered. This is in strong contrast to the case at room or high temperatures, where the experimental results have been well understood in the framework of the classical ballistic electron scattering.<sup>14</sup> The results indicate that at lower temperatures, the electron transport in the devices has

come into a new physical regime. We also discover very similar phenomena in the nanostructured artificial material. We propose a simple model, and show that the experimental results of the ballistic rectifiers and the nanomaterials can be qualitatively explained in a unified physical picture based on the quantum electron transport.

Both the ballistic rectifiers and the nanomaterials are fabricated from a modulation-doped  $\text{In}_{0.75}\text{Ga}_{0.25}\text{As}/\text{InP}$  heterostructure (details in Ref. 15), in which electrons are confined to a two dimensional electron gas (2DEG) in a 9 nm thick quantum well located 40 nm below the surface. The patterns are defined using standard electron beam lithography and wet chemical etching (details in Ref. 16). Figures 1 (a) and (b) show the scanning electron micrographs of a typical ballistic rectifier and a part of a typical nanomaterial measured in the experiments. The dark triangular areas are etched down through the 2DEG layer, and serve as artificial scatterers for the ballistic electrons. In both cases, there are four electrical contacts: left or source (S), right or drain (D), lower (L), and upper (U). The width of the source and drain channels of the ballistic rectifier, shown in Fig. 1 (a), is about 100 nm, while the width of the upper and lower channels is about 500 nm. The triangular antidot is situated away from the center of the cross junction, which results in pronounced nonlinear effects as will be discussed below. The nanomaterial, which we show the results from here, has a repetition period of 600 nm in the horizontal direction, and 300 nm in the vertical direction. Both the base and the height of the triangles are 150 nm. The device consists of a cross junction with four contacts, and the written pattern covers the whole area. The distance between the contacts is  $45 \mu\text{m}$  both between the source and the drain, and between the upper and the lower contacts. Without illumination, the 2DEG has the following parameters: carrier concentrations of  $4.5 \times 10^{15} \text{ m}^{-2}$  and  $4.7 \times 10^{15} \text{ m}^{-2}$ , and mobilities of  $45 \text{ m}^2/\text{Vs}$  and  $1.2 \text{ m}^2/\text{Vs}$ , at  $T = 0.3 \text{ K}$  and room temperature, respectively. Thus, the mean free path  $l_e$  varies from  $5 \mu\text{m}$  at 0.3 K to 140 nm at room temperature. At room temperature,  $l_e$  is shorter than but comparable to the distance between the triangular antidot and the source or drain channel in the ballistic rectifier, meaning that the electron transport is partially ballistic. Similarly, the electron transport within one “unit cell” of the artificial lattice in Fig. 1(b), which largely determines the transport properties of the whole nanomaterial, is also partially ballistic at room temperature. As the temperature is lowered, the electron transport in both the ballistic rectifier and one unit cell in the nanomaterial becomes purely ballistic.

The experiments are performed by applying a DC voltage,  $V_{SD}$ , between the source and drain and measuring the DC output voltage,  $V_{LU}$ , between the lower and upper contacts.<sup>17</sup> Figure 2 shows the temperature dependence of the ballistic rectifier. At room temperature,  $V_{LU}$  is negative, which is consistent with the results of our previous experiments,<sup>3,11</sup> which have been described by a model based on the classical ballistic transport.<sup>14</sup> The output remains negative as long as the temperature is above about 70 K. However, starting from about  $T = 200$  K, the curves show a clear trend of upward bending, and a pronounced output reversal is observed at temperatures below about 40 K. Even more surprisingly, when the temperature is below about 78 K, oscillatory behavior can be clearly identified.

Separate experiments show that lower temperatures are needed to observe output reversal if the sample is illuminated by an LED before the measurements. After the illumination, the electron concentration is increased by up to 30% and the electron Fermi wavelength becomes shorter. A number of devices with different geometric parameters (from half to about twice the size in Fig. 1) have also been measured, and the general trend is that the larger the device, the lower the temperature at which the output reversal starts to be seen. Both facts suggest that quantum effects play an important role in causing the reversed and oscillatory output. This may be expected because the width of the source and drain channels, from which the ballistic electrons are ejected, is comparable to the electron Fermi wavelength.

Reversed and oscillatory output from a ballistic rectifier was predicted very recently by Fleischmann and Geisel.<sup>18</sup> The mechanism was attributed to the large difference between the channel widths of the upward and downward electron transmissions from S and D in the ballistic rectifier, i.e., the gap between the triangular antidot and the edge of the upper channel is much narrower than the gap between the triangle and the edge of the lower channel. They argued that when the applied voltage is small, the number of occupied modes of lateral quantum confinement in the (lower) wider gap may increase because of the applied voltage, while the number of occupied modes in the (upper) narrower gap remains constant due to the larger energy separation of the lateral confinement energy levels. This gives rise to the “normal” rectifying effect ( $V_{LU} < 0$ ). When the applied voltage is high enough to open up a new mode in the upper gap, however, the output  $V_{LU}$  should undergo a change of sign, i.e., output reversal.

While the result predicted by the model appears to be in good agreement with the experimental results in Fig. 2, such mechanism for the output reversal does not seem to

exist in the nanomaterials shown in Fig. 1(b). This is because that in a nanomaterial, the width of the channel, which the electrons have to pass to transmit upwards after being ejected from a narrow gap between two neighboring triangles in a vertical column, is identical to the channel width of the downward electron transmission. As a result, the changes in the occupied lateral confinement modes in the channels of both upward transmissions and the downward transmissions are essentially identical. However, when measuring the nanomaterials with various geometric parameters, we observe very similar reversed as well as oscillatory output to that shown in Fig. 2. Figure 3 shows typical results measured from a nanomaterial, which are unexpected from the model in Ref. 18.

In Fig. 3, the output is “normal” at room temperature, which has been understood in the framework of the classical ballistic transport.<sup>12</sup> Output reversal starts to be seen at temperatures as high as 204 K. A blow-up of the curve at  $T = 4.2$  K clearly shows an oscillatory output.<sup>19</sup> Also, similar to the case of the ballistic rectifiers, the experiments show that the larger the gaps or the “lattice constants” of the artificial lattice, the lower the temperature at which output reversal starts to be seen. In samples with much larger gaps between neighboring triangles (not shown here), no output reversal is observed down to  $T = 4.2$  K. This again suggests that quantum effects play an important role. Furthermore, the striking similarities in the experimental results in the ballistic rectifiers and the nanomaterials suggest the existence of a common physical process that gives rise to the phenomena.

To understand the output reversal and the oscillatory output, we noticed that the width of the source and drain channels in the ballistic rectifier and the width of the gaps between neighboring triangles in a vertical column in the nanomaterial are all comparable to the electron Fermi wavelength, which is about 35 nm in our samples. By taking into account of the finite depletion depth at the etched device boundaries, the real widths of the lateral quantum confinement are even narrower than those shown in Fig. 1.

To simplify the presentation of our model, we first consider the artificial nanomaterial. At high temperatures, the transverse quantum confinement modes in the gaps between neighboring triangles in a vertical column cannot be well resolved due to the broad Fermi-Dirac distribution. The angular distribution of electrons ejected from a gap is not uniform but, to some extent, collimated,<sup>20,21,22,23</sup> as schematically shown in Fig. 4. The pattern of the angular distribution in the nanomaterial is tilted upwards a little because the geometry of each gap between the two neighboring triangles is asymmetric.<sup>23,24</sup> From the angular dis-

tribution, one anticipates that the triangular scatterer immediately on the right will deflect most of the electrons downwards, while fewer electrons can transmit upwards without being scattered by the triangle. This may appear to result in an accumulation of electrons in the lower contact, and consequently induce a negative output voltage  $V_{LU}$ . However, this certainly cannot happen if no voltage is applied to the nanomaterial, since there are always the same number of transmissions along the opposite directions under the equilibrium condition. As is shown by the model of the ballistic rectifier,<sup>14</sup> a nonzero output can only be generated by changes of the transmission coefficients caused by the applied voltage. For a finite negative  $V_{SD}$ , for example, the voltage drops, mainly at the openings and the exits of the gaps,<sup>25</sup> will cause an increase in the velocity components of the electrons along the S-D direction, while the velocity components in the perpendicular direction are virtually not affected. This leads to smaller ejection angles of the electrons with respect to the S-D axis, and therefore an overall narrower angular pattern of the electron flow from S, as shown in Fig. 4(b). Furthermore, the overall angular distribution of the ejected electrons should also level a bit as it tends to follow the direction of the electric field. Such a collimation effect induced by the applied voltage will clearly change the transmission coefficients, resulting in more downward deflections of the electrons by the triangular scatterer, and fewer upward transmissions. This leads to a “normal” negative output  $V_{LU}$  as observed at high temperatures in Fig. 3 (The probabilities for the electrons from L and U to transmit to the drain contact are not much affected because the electric field is only strong in the region very close to the gaps between neighboring triangles within a vertical column). If a positive  $V_{SD}$  is applied, the angular pattern of left-moving electrons from the gaps determines the net flow of carriers, and should be considered. Also in this case, the angular pattern becomes narrower and more leveled due to the applied electric field, and yields the same negative  $V_{LU}$ . This is also required by the geometric symmetry with respect to the L-U axis.

At sufficiently low temperatures, the transverse modes in the gaps become well resolved. It is rather complex to determine the number of occupied modes in the gaps, because while the electron transport between neighboring triangular antidots is ballistic, the transport over the whole material is not. Furthermore, both electron back scatterings and multiple reflections from the antidots also seriously influence the resistance. However, from the width of the gaps (about 100 nm) and the depletion depth (about 10 to 20 nm at each edge of the etched gaps), we estimate that there are between one and four occupied modes

at low temperatures. Separate resistance measurements on devices consisting of only a single narrow channel of similar width have confirmed the above estimate on the number of occupied modes. Similarly to the case of a quantum point contact in the adiabatic transport regime, each mode contributes to a specific angular pattern of electron flow from the gaps. The number of lobes (or branches) in the pattern of electron flow corresponds to the number of maximums in  $|\psi|^2$  (where  $\psi$  is the electron transverse wavefunction), as a direct result of the adiabatic transport. Therefore, for the  $N$ th transverse mode, the number of lobes is  $N$ . Such branch-like patterns of electron flow were recently imaged using a low-temperature scanning probe microscope.<sup>26,27</sup> In their experiments, additional fine fringes, separated by half the Fermi wavelength, were discovered on the branch-like patterns, which are caused by coherent constructive and destructive backscattering of the electron waves. In general, such effects of quantum phase coherence can be easily destroyed by increasing the temperature or applying a bias voltage<sup>29</sup>, which is the reason why the fine fringes were observed only at very low effective electron temperatures. However, the branch-like electron flow survived at biases up to at least 3 mV (corresponding to 30–40 K), because it is associated with the spacing between the transverse quantum confinement subband levels. In our experiments, since the reversed and oscillatory output is observed at up to about 150 K and quite large biases, where the phase coherence is unlikely to exist over the distance between neighboring triangles, only the branch-like electron flow is considered and will be shown below to result in the observed phenomena.

For simplicity, we assume that there is only one occupied mode at zero applied voltage, which corresponds to the angular pattern of the electron flow shown in Fig. 5(a), but the following discussion applies to other (if not too large) numbers of initially occupied modes. The angular distribution in Fig. 5(a) is narrower than that in Fig. 4(a) because of the lower temperature. We note that  $l_e$  is not longer than a few unit cells of the artificial lattice even at 4.2 K, implying that the electron transport within a unit cell should be, to a large extent, representative of the overall behavior of the nanomaterial. If a small negative source-drain voltage is applied, the voltage-induced collimation effect leads to a narrower and more leveled angular pattern of the electron flow, which is similar to the case at higher temperatures shown in Fig. 4(b). As a result, the downward transmissions of the electrons deflected by the triangle increase, which gives rise to a negative output  $V_{LU}$ . This explains the initial negative output voltage (or “normal” behavior) at low temperatures. If the

applied negative voltage is decreased further, the right-moving electrons from the left-hand side of a gap will eventually occupy the second lateral confinement mode,<sup>28</sup> which gives rise to a two-branch angular distribution, on top of the single-branch pattern of electron flow of the first occupied mode. In total, there are three lobes of electron flow as shown in Fig. 5(c). The widening of the angular distribution clearly results in an increased probability (or percentage) for the electrons to transmit upwards, and a reduced probability of the downward transmissions. As shown by a detailed model and analysis in Ref. 14 (see Eq. (6) and the discussions), the output of a ballistic rectifier is determined by the *relative* changes of the transmission coefficients,  $\Delta T/T$ , rather than the absolute values of the changes in the transmission coefficients  $\Delta T$ . This should be true for the artificial material as well, because of the similarities between a ballistic rectifier and a unit cell of the artificial material. Therefore, the increased probability (or percentage) for the electrons to transmit upwards and the reduced probability of the downward transmissions, which are discussed above and illustrated in Fig. 5(c), will lead to an increase in  $V_{LU}$  and may even cause the output reversal (from negative to positive) as observed in Fig. 3 in the intermediate  $V_{SD}$  range.

If the negative applied voltage is decreased further, the applied voltage or electric field should again cause the narrowing and leveling of the overall angular pattern of the electron flow as shown in Fig. 5(d). The right-moving electrons hence have more and more chance to be scattered downwards by the triangle on the right-hand side, and this contributes again to a decrease in  $V_{LU}$ . The voltage-induced collimation effect is more pronounced at lower temperatures, since the average kinetic energy of the electrons is smaller and it is easier to reduce the ejection angle of an electron at a given voltage drop across the gaps. At sufficiently low temperatures the downward bending of the curve may be strong enough to cause negative output again, and therefore gives rise to an overall oscillatory output, which is in good agreement with the experimental data in Fig. 3.

The electron transport in the ballistic rectifier is quite similar to that in the nanomaterial discussed above. At high temperatures, the collimation effect induced by a finite negative applied voltage narrows the angular distribution of the electrons ejected out of S, as shown in Fig. 4(d). This enhances the probability for the electrons to be deflected downwards by the triangular antidot, and decreases the probability of the upward electron transmissions, leading to the “normal” negative output  $V_{LU}$ . At sufficiently low temperatures, also similar to the case of the artificial nanomaterial, by decreasing the applied voltage  $V_{SD}$  from zero, the



angular distribution of the electrons ejected out of S changes alternately by subsequently narrowing as shown in Fig. 5(f), widening(g), narrowing (h), due to the interplay between the electric field induced collimation and the openings of additional lateral confinement modes in the source channel. This results in oscillatory modulations to the transmission probabilities for the electrons to be transmitted upwards and downwards, and hence leads to an oscillatory output  $V_{LU}$ .

Based on this model, it is easy to predict that at low temperatures the output reversal may well start showing up around  $V_{SD} = 0$ . In the above discussion, it is assumed that the Fermi energy at  $V_{SD} = 0$  lies well inbetween two transverse subbands, either in the source and drain channels of the ballistic rectifier or in the gaps between neighboring triangular antidots in a vertical column in the nanomaterial. In reality, it is possible that the Fermi energy is just below the bottom of the next subband. Because of the finite broadening of the subband as well as the Fermi-Dirac distribution, the occupation of the higher subband is not an abrupt process. In this case, any finite negative applied voltage may greatly enhance the population of the high subband, and result in the broadening of the angular distribution of the ejected electrons and hence a reversed output starting right from  $V_{SD} = 0$ . Experimentally, we indeed observe such a phenomenon, and the low-temperature curves in Figure 2 are such an example. Also, since the chance for the Fermi energy to be just below a transverse subband is relatively small, in most cases one should observe a “normal” negative output around  $V_{SD} = 0$ , which is indeed the case in our experiments where the devices are measured at different processes of cooling downs, which cause small variations in the electron concentration and therefore changes in the electron Fermi energy.

Apart from the similarities in the results of the ballistic rectifier and the nanomaterials, we notice that there are differences between the temperature dependences in Figs. 2 and 3. This is not surprising because of the noticeable differences between the ballistic rectifier and the nanomaterial. So far, we have only discussed the electron scattering within one unit cell of the nanomaterial. While a unit cell should largely represent some of the key transport properties of the whole nanomaterial, long trajectories of the ballistic electron over more than one unit cells also play an important role in the determination of the output voltage  $V_{LU}$ , especially when the mean free path is long at low temperatures. The analysis of the detailed influence of long trajectories of the inter-unit-cell scatterings is very complex and is not presented in this paper. Furthermore, as mentioned earlier, the large difference in the

channel widths between the upward and downward transmissions in the ballistic rectifier does not exist in the nanomaterial. Therefore, it is expected that the transport properties of the nanomaterial and the ballistic rectifier can well have different temperature dependence.

To conclude, we have investigated the electron transport in nanoscale ballistic rectifiers and nano-structured artificial materials, from the classical ballistic transport regime at room temperature down to a new regime at low temperatures. Reversed and oscillatory outputs are observed. We present a model based on the quantum and adiabatic electron transport, which explains the key phenomena that we have observed at low temperatures, and the similarities in the output from the ballistic rectifiers and the nanomaterials.

### Acknowledgments

The authors are grateful to L. Samuelson for constant support and W. Seifert for providing us the InP/InGaAs material. We wish to thank I. Maximov for the technical help and H. Q. Xu for the discussions. This work was supported by the Swedish Research Council, the Swedish Foundation for Strategic Research, and the European Commission through LTR research projects Q-SWITCH and NEAR.

---

\* Corresponding author. Email address: A.Song@umist.ac.uk

<sup>1</sup> For reviews, see C. W. J. Beenakker and H. van Houten, *Solid State Physics* **44**, 1 (1991); S. Datta, *Electronic Transport in Mesoscopic Systems* (Cambridge University Press, Cambridge, 1995).

<sup>2</sup> A. Lorke, S. Wimmer, B. Jager, J. P. Kotthaus, W. Wegscheider, and M. Bichler, *Physica B* **249-251**, 312 (1998).

<sup>3</sup> A. M. Song, A. Lorke, A. Kriele, J. P. Kotthaus, W. Wegscheider, and M. Bichler, *Phys. Rev. Lett.* **80**, 3831 (1998).

<sup>4</sup> H. Linke, W. Sheng, A. Löfgren, H. Q. Xu, P. Omling, and P.E. Lindelof, *Europhys. Lett.* **44**, 341 (1998).

<sup>5</sup> H. Linke, T. E. Humphrey, A. Löfgren, A. O. Sushkov, R. Newbury, R. P. Taylor, and P. Omling, *Science* **286**, 2314 (1999).

- <sup>6</sup> D. R. S. Cumming and J. H. Davies, *Appl. Phys. Lett.* **69**, 3363 (1996).
- <sup>7</sup> K. S. Novoselov, Y. V. Dubrovskii, V. A. Sablikov, D. Y. Ivanov, E. E. Vdovin, Y. N. Khanin, V. A. Tulin, D. Esteve, and S. Beaumont, *Europhys. Lett.* **52**, 660 (2000)
- <sup>8</sup> K. Hieke and M. Ulfward, *Phys. Rev. B* **62**, 16727 (2000).
- <sup>9</sup> H. Q. Xu, *Appl. Phys. Lett.* **78**, 2064 (2001); **80**, 853 (2002); I. Shorubalko, H. Q. Xu, I. Maximov, P. Omling, L. Samuelson, and W. Seifert, *ibid.* **79**, 1384 (2001); I. Shorubalko, H. Q. Xu, I. Maximov, D. Nilson, P. Omling, L. Samuelson, and W. Seifert, *IEEE Electron Device Letters*, **23**, 377 (2002)
- <sup>10</sup> L. Worschech, B. Weidner, S. Reitzenstein, and A. Forchel, *Appl. Phys. Lett.* **78**, 3325 (2001); L. Worschech, H. Q. Xu, A. Forchel, and L. Samuelson, *ibid.* **79**, 3287 (2001)
- <sup>11</sup> A. M. Song, P. Omling, L. Samuelson, W. Seifert, I. Shorubalko, and H. Zirath, *Jpn. J. Appl. Phys.* **40**, L909 (2001).
- <sup>12</sup> A. M. Song, P. Omling, L. Samuelson, W. Seifert, I. Shorubalko, and H. Zirath, *Appl. Phys. Lett.* **79**, 1357 (2001).
- <sup>13</sup> H. Ueno, K. Moriyasu, Y. Wada, S. Osako, H. Kubo, N. Mori, and C. Hamaguchi, *Jpn. J. Appl. Phys.* **38**, 332 (1999).
- <sup>14</sup> A. M. Song, *Phys. Rev. B* **59**, 9806 (1999).
- <sup>15</sup> P. Ramvall, N. Carlsson, P. Omling, L. Samuelson, W. Seifert, M. Stolze, and Q. Wang, *Appl. Phys. Lett.* **68**, 1111 (1996).
- <sup>16</sup> I. Maximov, Q. Wang, M. Graczyk, P. Omling, L. Samuelson, W. Seifert, and I. Shorubalko, In *Proc. of 11<sup>th</sup> Internat. Conference on InP and Related Materials, 1999*, (Institute of Electrical and Electronics Engineers, Davos, Switzerland), p. 237.
- <sup>17</sup> Since the device fabrication cannot be perfect, the ballistic rectifier and the artificial material are not perfectly symmetric along the U-L axis. This causes that the observed output between the lower and upper contacts,  $V_{\text{output}}$ , at a given applied voltage  $V_{SD}$  is different from the output at  $-V_{SD}$ . To eliminate this effect and focus on the nonlinear effect induced by the artificial triangular antidot, we always extracted the effective output,  $V_{LU}(V_{SD}) = [V_{\text{output}}(+V_{SD}) + V_{\text{output}}(-V_{SD})]/2$ , and reported it throughout the paper. This is also equivalent to the case of applying an AC signal and measure the DC output. Note also that due to the series resistances of the ohmic contacts and the broad 2DEG regions between the contacts and source/drain channels, the real voltage drop on the device is much less than  $V_{SD}$ , which also depends on

temperature.

- <sup>18</sup> R. Fleischmann and T. Geisel, Phys. Rev. Lett. **89**, 16804 (2002).
- <sup>19</sup> The different voltage ranges of the different curves shown in Fig. 3 are due to the fact that the experiments were carried out by sweeping the source-drain current to a fixed range. At lower temperatures, the overall resistances were lower, resulting in smaller voltage ranges.
- <sup>20</sup> C. W. J. Beenakker and H. van Houten, Phys. Rev. B **39**, 10445 (1989).
- <sup>21</sup> L. W. Molenkamp, A. A. M. Staring, C. W. J. Beenakker, R. Eppenga, C. E. Timmering, and J. G. Williamson, C. J. P. M. Harmans, C. T. Foxon, Phys. Rev. B **41**, 1274 (1990).
- <sup>22</sup> K. L. Shepard, M. L. Roukes, and B. P. Van der Gaag Phys. Rev. Lett. **68**, 2660 (1992).
- <sup>23</sup> R. I. Hornsey, J. Appl. Phys. **79**, 9172 (1996)
- <sup>24</sup> R. Akis, D. K. Ferry and J. P. Bird, Phys. Rev. B **54**, 17705 (1996).
- <sup>25</sup> S. Ulreich and W. Zwerger, Superlattices Microstruct. **23**, 719 (1998).
- <sup>26</sup> M. A. Topinka, B. J. LeRoy, S. E. J. Shaw, E. J. Heller, R. M. Westervelt, K. D. Maranowski, and A. C. Gossard, Science **289**, 2323 (2000).
- <sup>27</sup> R. Crook, C. G. Smith, M. Y. Simmons, and D. A. Ritchie, J. Phys. Cond. Mat. **12**, L735 (2000).
- <sup>28</sup> L. P. Kouwenhoven, B. J. van Wees, C. J. P. M. Harmans, J. G. Williamson, H. van Houten, C. W. J. Beenakker, C. T. Foxon and J. J. Harris, Phys. Rev. B **39**, 8040 (1989).
- <sup>29</sup> J. J. Lin and J. P. Bird, J. Phys.: Condens. Matter **14**, R501 (2002)

## Figures

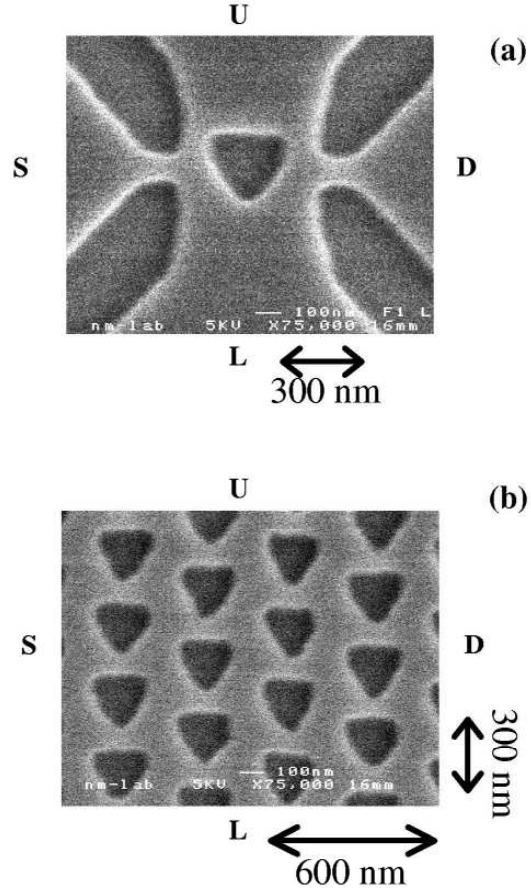


FIG. 1: Scanning electron micrographs of (a) the ballistic rectifier and (b) the artificial nanomaterial measured in the experiments. The dark triangular areas are etched down through the layer of the two-dimensional electron gas, and serve as artificial scatterers for the ballistic electrons. In both cases, there are four electrical contacts: left or source (S), right or drain (D), lower (L), and upper (U).

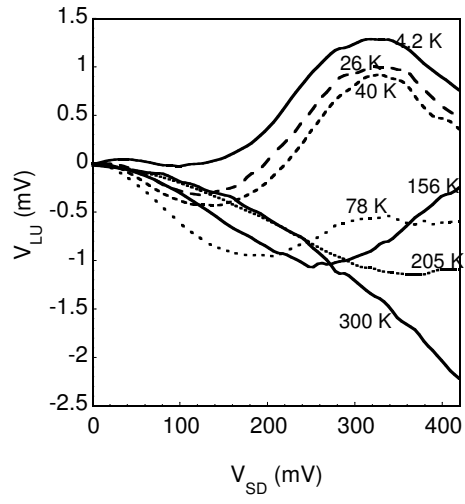


FIG. 2: The output of the ballistic rectifier,  $V_{LU}$ , as functions of the applied source-drain voltage,  $V_{SD}$ , measured at different temperatures.

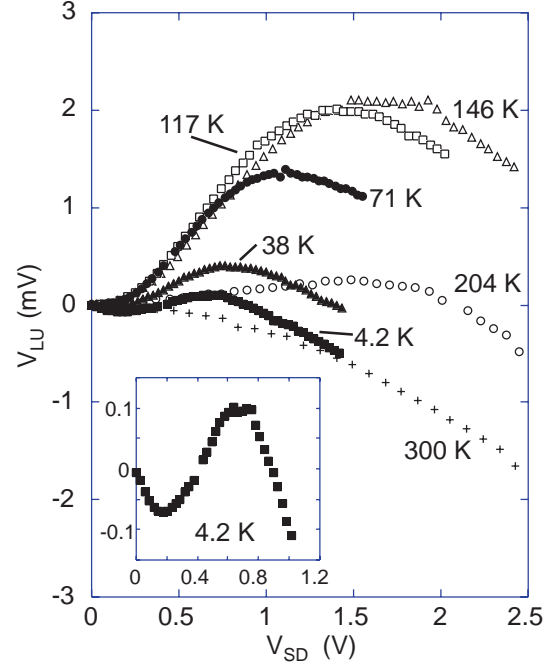


FIG. 3: The output of the artificial nanomaterial  $V_{LU}$  as functions of the applied source-drain voltage  $V_{SD}$  measured at different temperatures. The inset is a magnification of the 4.2 K data.



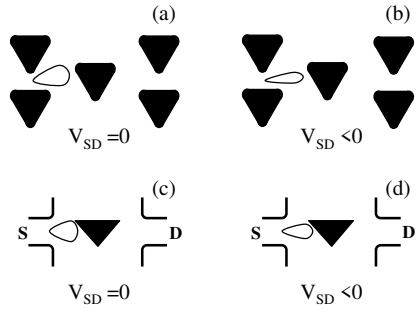


FIG. 4: Schematic model of the classical ballistic electron transport at *high temperatures*, for the “normal” negative output of the nanomaterial, shown in (a) and (b), and the ballistic rectifier, shown in (c) and (d). Note that the patterns of the angular distribution in the nanomaterial are tilted a little bit upwards because the geometry of each gap between the two neighboring triangles is asymmetric.

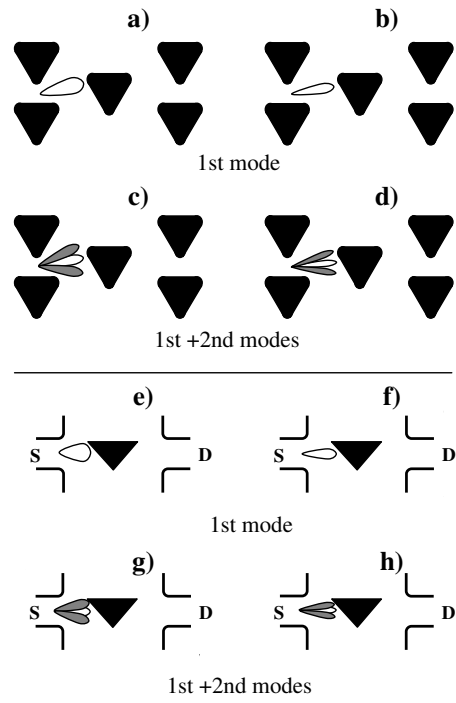


FIG. 5: Schematic model for the output reversal and oscillatory output, in one unit cell of the artificial nanomaterial (a)-(d) and in the ballistic rectifier (e)-(h) at *low temperatures*. As an example, suppose that there is only one lateral confinement mode occupied in the narrow gaps between neighboring triangles in a vertical column when the applied voltage  $V_{SD}$  is zero. As a result of the adiabatic transport at low temperatures, the electrons ejected out of the gaps have a narrow (rather than uniform) angular distribution (a). With decreasing  $V_{SD}$ , the angular distribution first becomes narrower due to the collimation effect induced by applied electric field, and also becomes more horizontal to follow the direction of the electric field, as shown in (b). By decreasing  $V_{SD}$  further, eventually the second lateral confinement mode becomes occupied, which gives rise to a two-branch angular distribution, on top of the single-branch pattern of electron flow of the first occupied mode. In total, there are three lobes in the electron flow (c). The total angular distribution will become narrower again with continuing decreasing  $V_{SD}$  because of the voltage-induced collimation effect (d). Overall, by decreasing the applied voltage  $V_{SD}$  from zero, the angular distribution of the electrons ejected out of the gaps changes alternately by subsequentially narrowing (b), widening(c), narrowing (d)... Consequently, both the upward and downward transmission probabilities for the electrons ejected from the gaps are oscillatory functions of  $V_{SD}$ , and this induces the oscillatory output  $V_{LU}$  as shown in Fig. 3. Similar to the case of the artificial nanomaterial shown in (a)-(d), by decreasing  $V_{SD}$  applied to the ballistic rectifier from zero, the angular distribution of the electrons ejected out of S changes alternately by subsequentially narrowing (f), widening(g), narrowing (h),..., because of the interplay between the voltage-induced collimation and the openings of additional lateral confinement modes in the source channel.